CHEMISTRY OF MATERIALS

Article

pubs.acs.org/cm

Quantum Dot Color-Converting Solids Operating Efficiently in the kW/cm^2 Regime

Cai-Feng Wang,[†] Fengjia Fan,[†] Randy P. Sabatini, Oleksandr Voznyy, Kristopher Bicanic, Xiyan Li, Daniel P. Sellan, Mayuran Saravanapavanantham, Nadir Hossain, Kefan Chen, Sjoerd Hoogland, and Edward H. Sargent*

Department of Electrical and Computer Engineering, University of Toronto, 10 King's College Road, Toronto, Ontario M5S 3G4, Canada

Supporting Information

ABSTRACT: With rapid progress in the use of colloidal quantum dots (QDs) as light emitters, the next challenge for this field is to achieve high brightness. Unfortunately, Auger recombination militates against high emission efficiency at multiexciton excitation levels. Here, we suppress the Auger-recombination-induced photoluminescence (PL) quantum yield (QY) loss in CdSe/CdS core−shell QDs by reducing the absorption cross section at excitation wavelengths via a thin-shell design. Studies of PL vs shell thickness reveal that thin-shell QDs better retain their QY at high excitation intensities, in stark contrast to thicker-shell QDs. Ultrafast transient absorption spectroscopy confirms increased Auger recombination in thicker-shell QDs under equivalent external excitation intensities. We then further grow a thin ZnS layer on thin-shell QDs to serve as a higher conduction band barrier; this allows for better passivation and exciton confinement, while providing transparency at the excitation wavelength. Finally, we develop an isolating silica matrix that acts as a spacer between dots, greatly reducing interdot energy transfer that is otherwise responsible for PL reduction in QD films. This results in the increase of film PL QY from 20% to 65% at low excitation intensity. The combination of Auger reduction and elimination of energy transfer leads to QD film PL QY in excess of 50% and absolute power conversion efficiency of 28% at excitation powers of 1 kW/cm^2, the highest ever reported for QDs under intense illumination.

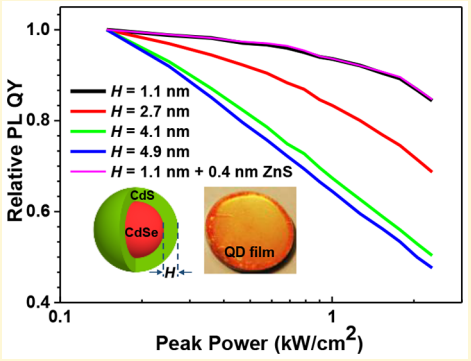

INTRODUCTION

Semiconductor quantum dots (QDs) are used as light-emitting materials in commercial lighting and display technologies owing to their favorable electronic and optical properties: advantages include a size-tunable full-visible-spectrum emission, high color purity, and high photoluminescence quantum yields (PL QYs).[1] Thanks to improved techniques in thermal management and oxygen- and moisture-free encapsulation, QDs are used as phosphors in applications such as televisions and portable electronic devices.[1,2] These applications have so far been limited to operate at emission intensities at which multicarrier recombination mechanisms do not degrade emission efficiencies.

Newer large-area displays such as high-power projectors will require more intense light output. In these operating regimes, each QD will contain multiple excitons, giving rise to Auger recombination, a nonradiative process that reduces PL efficiency.[3,4] This nonradiative process is enhanced by colocalization of the electron and hole in a small volume. In quantum-confined systems, momentum conservation is relaxed, and Auger recombination is accelerated compared to bulk counterparts.[5]

In the past decade, significant efforts have been made to investigate and suppress multiexciton Auger recombination in QDs. Two strategies have been executed: wave function delocalization[6,7] and graded shell growth.[8,9] In the first case, the exciton wave function is expanded by growing QDs of larger size or use of a thick shell with small band-offsets between core and shell. This, unfortunately, also slows radiative decay, leaving the ratio of radiative-to-nonradiative rates barely affected. Increased absorption cross section due to the addition of large shells results in a faster exciton generation rate at any given excitation intensity. Two-photon correlation measurements of single dots with graded shells have shown reduced Auger recombination rates;[10] however, such dots suffer from low single exciton quantum yields, and thus only marginal benefit has been demonstrated in LED devices.[11]

For the practical application of QDs as an alternative to conventional phosphors, it is also imperative to preserve their high emission efficiencies in the solid state. When QDs are condensed into films, however, PL quenching is commonly observed and is more pronounced in thin-shell QDs, mainly owing to QD aggregation and energy transfer among neighboring QDs.[12−14] In light of this challenge, QDs

Received: January 13, 2017
Revised: May 26, 2017
Published: May 31, 2017

DOI: 10.1021/acs.chemmater.7b00164
Chem. Mater. XXXX, XXX, XXX−XXX

embedded in various polymeric and inorganic matrices have been developed.[15−20] The matrix materials separate and further stabilize QDs, while providing QDs with improved processability. Conventionally, thick-shell QDs are employed in such nanocomposites to provide high emission efficiencies.[21] Despite great advances in this field, the PL performance of the nanocomposites at high-power excitation has yet to be explored.

Here we demonstrate a new and efficient approach to avoid Auger-recombination-induced PL QY loss. We showcase our advance in red QD phosphors excited using the high-energy blue light source. We show first that desensitization by reducing the absorption cross section at the optical pump wavelength is an efficient approach to avoid Auger recombination in QDs. This conceptually straightforward solution to the Auger problem creates a new and significant challenge from the point of view of materials synthesis: a new strategy is now required to turn off energy transfer among thin-shell QDs in solid state, and to preserve excellent surface passivation at the same time. We, therefore, develop a transparent and isolative matrix that further stabilizes and efficiently separates the thin-shell QDs within solid films, thereby turning off energy transfer. The combination of Auger reduction and elimination of energy transfer is directly responsible for our ability to maintain high film PL QY under intense optical excitation.

EXPERIMENTAL SECTION

Chemicals. Cadmium oxide (CdO, >99.99%), zinc acetate dihydrate ($Zn(AC)_2{\cdot}2H_2O$, 99.99%), sulfur powder (S, >99.5%), selenium powder (Se, >99.99%), oleylamine (OLA, 80−90%), octadecene (ODE, 90%), oleic acid (OA, 90%), trioctylphosphine (TOP, 90%), trioctylphosphine oxide (TOPO), octadecylphosphonic acid (ODPA, 97%), 1-octanethiol (>98.5%), (3-mercaptopropyl)-trimethoxysilane (MPS, 95%), tetramethylammonium hydroxide solution (Me_4NOH, 25 wt % in methanol), and poly(methyl methacrylate) (PMMA, average M_w of ∼996,000) were purchased from Sigma-Aldrich and used without further purification.

Synthesis of Cd-oleate and Zn−OLA Complex. 2.98 g of CdO was fully dissolved in 40 mL of oleic acid at 170 °C under vacuum. 2.45 g of $Zn(AC)_2{\cdot}2H_2O$ was dissolved in OLA at 170 °C under vacuum until a clear light pink solution was obtained.

Synthesis of CdSe Core QDs. CdSe QDs were synthesized according to a modified method reported previously.[22] Typically, 240 mg of CdO, 24 g of TOPO, and 1.12 g of ODPA were mixed in a Schlenk flask (100 mL). The mixture was heated to 150 °C for 0.5 h under vacuum with continuous stirring. Then the system was refilled with N_2 and heated at 320 °C for 2 h. Subsequently, 4 mL of TOP was injected into the Schlenk flask, and the resulting mixture was further heated to 380 °C. Upon reaching 380 °C, 2 mL of TOP solution containing selenium (60 mg mL^{-1}) was injected into the system. CdSe QDs with the first excitonic peak at 586 nm were formed after about 2 min growth. Finally, the reaction was terminated by cooling and adding acetone. The resultant CdSe QDs were redispersed in hexane for shell growth.

CdS and ZnS Shell Growth on CdSe Cores. The shell growth was carried out as described previously.[23] CdSe core QDs were quantified by measuring absorbance ($A_{1st\text{-}exciton\text{-}peak}$) at exciton peak (586 nm) in a cuvette with a path length of 1 mm. A hexane solution of CdSe core QDs (8.8 mL, $A_{1st\text{-}exciton\text{-}peak}$ = 1) was mixed with oleylamine (OLA, 12 mL) and octadecene (ODE, 12 mL) in a 250 mL Schlenk flask. The mixture was heated to 100 °C under vacuum to remove hexane. The desired amounts of as-prepared Cd-oleate and octanethiol, respectively, were diluted in ODE, respectively, and then were injected simultaneously and continuously into the system at a rate of 12 mL h^{-1} while ramping the system temperature from 100 to 310 °C. Different amounts of Cd-oleate (1, 3, 6, and 7.5 mL) and octanethiol (106, 320, 640, 800 μL) were used for growth of different shell thickness.

To further grow ZnS shell on CdSe/CdS QDs, the above solution was cooled down to 290 °C. 1.5 mL of as-prepared Zn−OLA diluted in 10.5 mL of ODE was mixed with 0.03 g of sulfur dissolved in 2 mL of OLA. The mixture was slowly and continuously injected into the system for 1 h at 290 °C. After injection, the solution was annealed at 290 °C for 10 min, followed by an injection of 4 mL of oleic acid (OA) and further annealing for 10 min. The reaction was terminated by cooling and adding acetone at 80 °C. The resultant CdSe/CdS/ZnS QDs were purified by 3 cycles of centrifugation at 6000 rpm, redispersion in hexane, and precipitation by acetone. The final core−shell−shell CdSe/CdS/ZnS QDs were redispersed in toluene ($A_{1st\text{-}exciton\text{-}peak}$ = 2.5).

Synthesis of QD/Silica Composites. QD/silica composites were prepared according to a modified literature method.[24] QDs in toluene solution (400 μL, $A_{1st\text{-}exciton\text{-}peak}$ = 2.5) were precipitated by a solvent mixture of acetone and methanol, and separated by centrifugation at 6000 rpm. The precipitate was redispersed in 15 mL of tetrahydrofuran (THF), and then mixed with 200 μL of MPS in a three-neck flask under N_2. After 4 h of mild stirring, 60 mL of solvent mixture (THF:ethanol = 35:25 v:v) with pH of 9−10 (adjusted by 25 wt % of tetramethylammonium hydroxide in methanol solution) was added to the mixture. After 2 h of mild stirring, the solution was gently heated to 60 °C for 30 min, and then 600 μL of MPS was added. After maintaining the temperature at 60 °C for 5 min, the mixture was cooled to room temperature and stirred overnight. The resulting solution was condensed to ca. 20 mL by evaporation at room temperature, extracted with hexane, and then washed by ethanol/hexane (v/v = 1:10) several times. A homogeneous and transparent sol−gel solution was obtained, which was finally dispersed in 1 mL of ethanol. Films were prepared by spin-coating or drop-casting the sol−gel solution on diverse substrates including glass and polished aluminum disks, annealed at ca. 60 °C for 4 h for further gelation and cross-linking, further dried under vacuum for 2 days, and then stored in air.

Preparation of QD/PMMA Composites. 100 μL of toluene solution of QDs (A = 2.5) was mixed with 100 mg of PMMA in chloroform. The resulting solution was directly cast onto the glass to form a film, which was dried under vacuum overnight.

Characterizations. TEM images were taken by JEOL 2010, with an acceleration voltage of 200 kV. UV−vis absorption measurements were performed on a PerkinElmer Lambda 950 UV−vis−NIR spectrophotometer. The absorption (%) was calculated as 100% − transmission (T%). Photoluminescence (PL) spectroscopy and PL decay measurements were carried out on the Horiba Fluorolog TCSPC system with an iHR 320 monochromator and a PPO·900 detector. An integrating sphere was used for film and solution PL QY measurements.

For transient absorption spectroscopy, a regeneratively amplified Yb:KGW laser (Light Conversion, Pharos) at a 5 kHz repetition rate was used to produce femtosecond laser pulses. The pump pulse (570 or 442 nm) was generated by sending a portion of the 1030 nm fundamental to an optical parametric amplifier (Light Conversion, Orpheus). Both the pump pulse and probe (fundamental) were directed into an optical bench (Ultrafast, Helios), where a sapphire crystal was used to generate a white-light continuum from the fundamental. The time delay (time resolution ∼350 fs) was adjusted by delaying the probe pulse optically, with exponentially increasing time steps. Every other pump pulse was blocked by a chopper, and each probe pulse was measured by a CCD after dispersion by a grating spectrograph (Ultrafast, Helios). Samples were kept in a 1 mm cuvette and translated at 1 mm/s. Kinetic traces were fit to a sum of exponential decays. The power conversion efficiency (power in/power out) was measured under a pulsed pump (300 μs, 60 Hz) from a high power pulsed laser diode system providing in excess of 2 kW/cm^2 peak intensities at a wavelength of 442 nm. Using a lens system the collection was focused on an OPHIR PD300-3W photodiode with a 9 mm aperture.

DOI: 10.1021/acs.chemmater.7b00164
Chem. Mater. XXXX, XXX, XXX−XXX

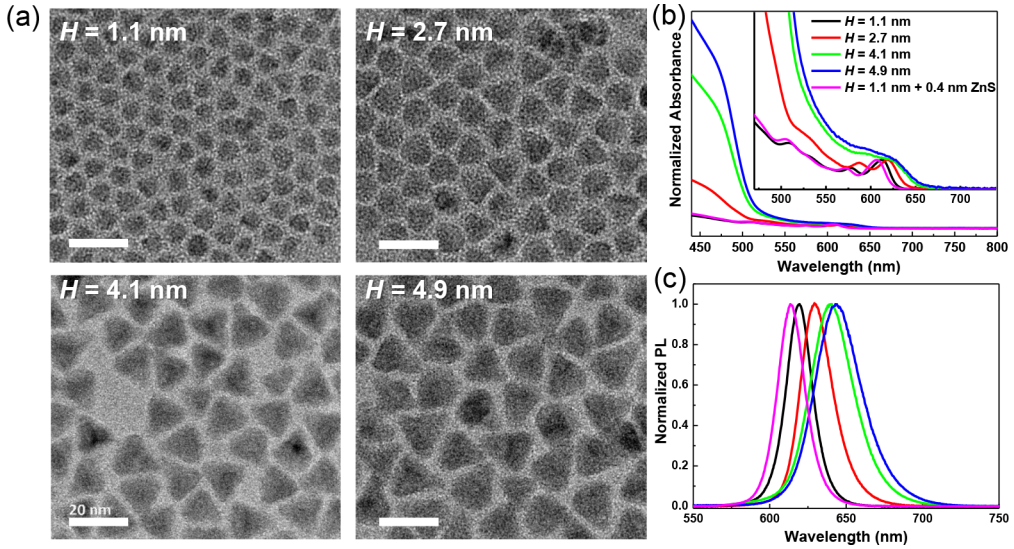

Figure 1. (a) TEM images of CdSe/CdS QDs with increasing shell thickness of H = 1.1, 2.7, 4.1, and 4.9 nm (scale bar: 20 nm). (b) The ground state absorbance spectra and (c) PL spectra for toluene solutions of different core−shell CdSe/CdS QDs (H = 1.1, 2.7, 4.1, and 4.9 nm) and CdSe/CdS(1.1 nm)/ZnS(0.4 nm) QDs.

Absolute Excitation Rate Estimation. To illustrate how the absorption cross sections and absolute excitation rates affect the PL QY and then the brightness/effective emission rates of different samples, we estimated the absolute excitation rates r_{ex} according to the following equation:

$$r_{ex} = J_{in}\sigma \quad (1)$$

where J_{in} and σ are the incident light flux and absorption cross section, respectively.

The absorption cross sections of the 4.1 nm shell dots were measured by following an existing method (eq 2):[25]

$$\sigma = \frac{2.303A}{cl} \quad (2)$$

where σ is absoprtion cross section of QDs, A is absorbance of QD in hexane dispersion at a certain wavelength, c is number of nanocrystals per cm^3, and l is light path length of the cuvette in units of cm.

400 μL of QDs dispersion with known absorbance was digested in nitric acid and diluted to 10 mL of aqueous solution. Inductively coupled plasma optical emission spectroscopy (ICP-OES) (Optima 7300 ICP AES) was applied to determine the total amount of Cd atoms (N_{total}), and the single dot Cd atom numbers were estimated from the volume of the CQDs (N_{single}), which were determined from the TEM images by assuming that they possess a conical shape. The diameter and height are the shortest edge length and tallest height of the triangle, respectively. c was calculated by following the equation. The 20% error bars come from the uncertainty in determination of QD volume.

$$c = \frac{N_{total}}{0.4N_{single}} \quad (3)$$

The absorption cross sections of other core−shell QDs were estimated by comparing the absorbance at 442 nm after normalizing the first exciton peak absorbance.

RESULTS AND DISCUSSION

Syntheses, Morphologies, and Optical Characterizations of QDs. CdSe/CdS QDs were synthesized according to previously reported methods;[23] modifications are detailed in the Experimental Section (Figure S1). Varying amounts of Cd-oleate and octanethiol were used as precursors to prepare CdS shells of different thicknesses on CdSe cores with a mean size of 4.6 nm (Figure S2). A series of CdSe/CdS QDs with increasing average diameter of 6.8, 9.9, 12.8, and 14.4 nm were prepared with corresponding shell thicknesses (H) of 1.1, 2.7, 4.1, and 4.9 nm, respectively, as determined by transmission electron microscopy (TEM) (Figures 1a and S3−S6, Table S1). A thin layer of ZnS (0.4 nm) was further grown on 1.1 nm CdS-shelled QDs to provide doubly shelled QDs (Figure S7).

To compare the relative core/shell absorption of these QDs at 442 nm, the optical pump wavelength for five spectroscopic experiments in this study, the ground state absorption spectra for dilute solutions of QDs in toluene were normalized with absorbance (A) at the exciton peak since the same core size was used in all samples. As shown in Figure 1b, the core-to-shell absorption ratio decreases as the shell thickness increases. With an increase in shell thickness, the absorption edge and PL peak shift to longer wavelengths as a result of electron wave function delocalization in the CdS shell (Figures 1b and 1c).[26] Correspondingly, the full width at half-maximum (fwhm) of PL peak varies from 20 to 36 nm (Figure 1c, Table S1). The broadening of the emission spectra is a commonly observed consequence of thick shell growth.[27−29] This spectral broadening is attributed to increased size and shape variations, increased exciton−phonon coupling, and spectral diffusion.[30] The PL QYs of the QD solutions pumped at 442 nm with a power density of 7×10^{-5} W/cm^2 were measured using the absolute measurement method,[31] and were determined to be in the range of 46−74% (Table 1). The thin ZnS shell grown on CdSe/CdS(1.1 nm) QDs serves as a higher conduction band barrier, allowing stronger exciton confinement and also better passivation (i.e., eliminating core surface dangling bonds that cause nonradiative trap recombination), while providing transparency at the excitation wavelength.

Photoluminescence of QDs under High Power. To evaluate the potential of these QDs as high-intensity phosphors, we employed a 442 nm pulsed laser (300 μs, 60 Hz), providing in excess of 2.5 kW/cm^2 peak intensities. We photoexcited the QDs at high intensities while monitoring PL QY. These pulsed photoexcitation conditions are similar to those in high-intensity projection phosphors which are immobilized on rotating disks and are excited sequentially to avoid overheating.

DOI: 10.1021/acs.chemmater.7b00164
Chem. Mater. XXXX, XXX, XXX−XXX

Table 1. PL QY and PL Lifetimes of CdSe/CdS QDs with Different Shell Thickness (H = 1.1, 2.7, 4.1, and 4.9 nm), CdSe/CdS(1.1 nm)/ZnS(0.4 nm) QDs, and Their QD/Silica and QD/PMMA Composites

	PL QY (%) under 7×10^{-5} W/cm^2		PL lifetime (ns)	
sample	solution	film	solution	film
CdSe/CdS(1.1 nm)	46	18	11.9	7.2
CdSe/CdS(2.7 nm)	74	58	27.5	22.6
CdSe/CdS(4.1 nm)	65	40	49.1	43.1
CdSe/CdS(4.9 nm)	61	45	76.2	54.4
CdSe/CdS(1.1 nm)/ZnS(0.4 nm)	60	20	16.8	8.7
QD/silica composites[a]		65		21.5
QD/PMMA composites[a]		30		9.6

[a]CdSe/CdS(1.1 nm)/ZnS(0.4 nm) QDs were used for preparation of composite samples.

Solution samples were used in these measurements to avoid charge carrier and exciton transfer which would decrease the PL QY. The PL QYs at peak pump powers varying from 0.1 to 2.5 kW/cm^2 were determined via combined measurements: the absolute values were measured at 1 kW/cm^2, and those at other peak powers were obtained by scaling the output:input power ratio relative to 1 kW/cm^2; the absorption of all solution samples was adjusted to the same value (ca. 80%) at the pump wavelength to enable fair comparison prior to use. The dependences of the absolute and relative PL QY on pump power are plotted in Figures 2a and 2b, respectively. The absolute PL QYs measured at low peak powers mainly depend on the surface passivation (Table 1 and Figure 2a), while the impact of Auger recombination can be clearly seen in the pump-power scaling of relative PL QY (Figure 2b). 2.7 nm CdS shell and 1.1 nm CdS with extra ZnS shell QDs show much higher PL QY than other samples at 0.1 kW/cm^2 because of good passivation and the absence of Auger recombination induced emission quenching. The slope of relative PL QY in 4.9 nm CdS shelled QDs is much steeper than that in 1.1 nm CdSe shelled QDs (Figure 2b), indicating that the main causes of low PL QY at 0.1 kW/cm^2 in the two types QDs are different: the first is pump-power-dependent Auger recombination quenching, and the latter is poor passivation.

To facilitate a better comparison among QDs with different shell thickness, we converted the pump powers to the absolute excitation rates (Figures 2c and 2d). Due to efficient shell sensitization, the excitation rates in thicker-shell QDs are higher than those in thinner-shell QDs at a given pump power. In the thinnest CdS-shelled QDs, the PL QY roll-off becomes significant only when the excitation rate exceeds 0.01 ns^{-1} per dot. However, in the thickest-shell QDs, the excitation rate is much higher than the above value, even at the lowest excitation power (0.1 kW/cm^2). This results in significant PL quenching across the measurement range. The bandgap of the ZnS shell is large and is not photoexcited by blue photons: for this reason, the excitation rate is not impacted by ZnS shell growth, and doubly shelled QDs show similar roll-off in relative PL QY at high pump power. Specifically, CdSe/CdS(1.1 nm)/ZnS(0.4 nm) at 2 kW/cm^2 pump power maintain an over 50% absolute PL QY as a result of good passivation and enlarged power onset for Auger recombination, afforded by the minimized sensitization.

Transient-Absorption Spectroscopy. Ultrafast transient-absorption (TA) spectroscopy was employed to investigate exciton population and decay dynamics.[32−35] To compare the carrier dynamics in QDs with different shell thicknesses in a controlled manner, we photoexcited the QDs at 570 nm, where the CdS shell does not absorb photons. The transient spectra for core-pumped QDs are presented in Figure 3a as $\Delta A/$

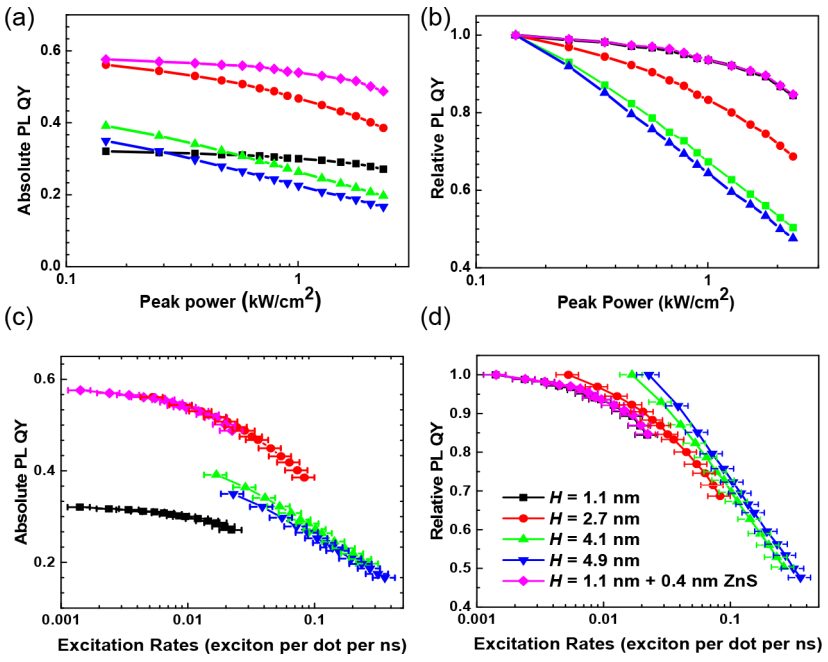

Figure 2. Dependence of (a, c) absolute solution PL QYs and (b, d) relative solution PL QYs on (a, b) pump power and (c, d) excitation rates for different core−shell CdSe/CdS QDs (H = 1.1, 2.7, 4.1, and 4.9 nm) and CdSe/CdS(1.1 nm)/ZnS(0.4 nm) QDs. The 20% error bar in excitation rate comes from the uncertainty in QD volume determination. Since nonradiative Auger recombination is much faster than the radiative recombination, keeping a low excitonic occupancy for single exciton radiation is beneficial to achieve high PL QY.

DOI: 10.1021/acs.chemmater.7b00164
Chem. Mater. XXXX, XXX, XXX−XXX

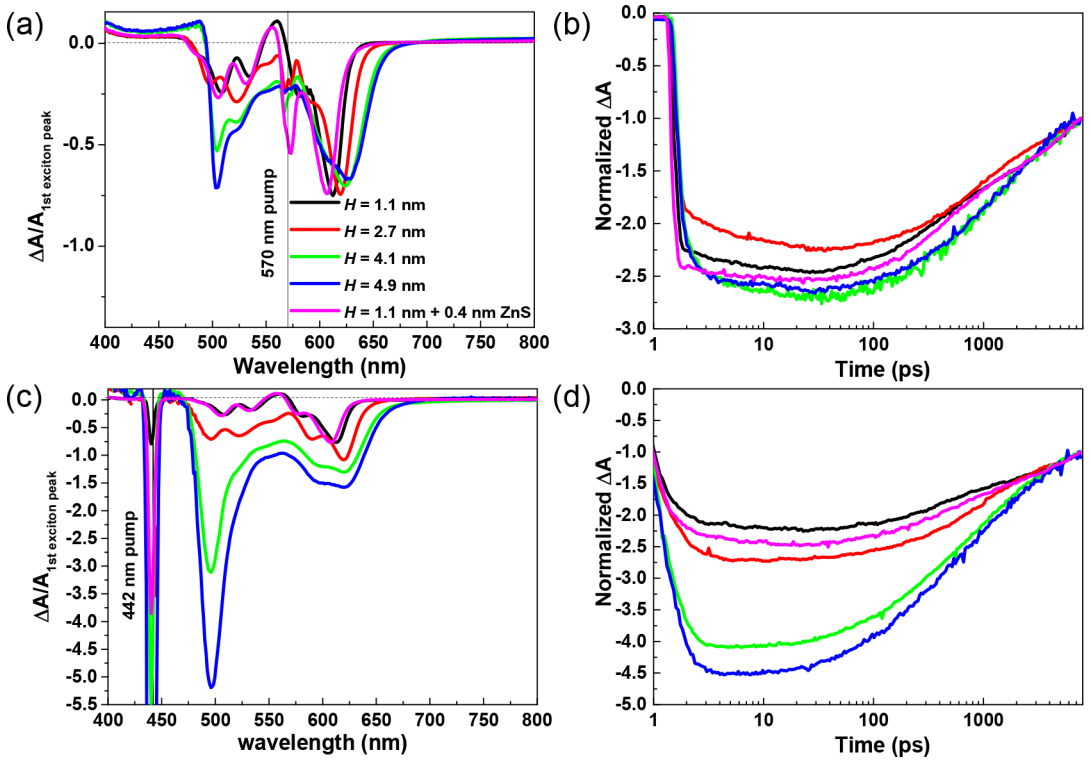

Figure 3. TA characterization for the solutions of core−shell CdSe/CdS QDs (H = 1.1, 2.7, 4.1, and 4.9 nm) and CdSe/CdS(1.1 nm)/ZnS(0.4 nm) QDs: (a) state filling of QDs with core-only pump at 570 nm at 50 ps (530 J/cm^2) and (b) corresponding time trace of exciton peak decay; (c) state filling of QDs with both core and shell pump at 442 nm at 50 ps (400 J/cm^2) and (d) corresponding time trace of exciton peak decay.

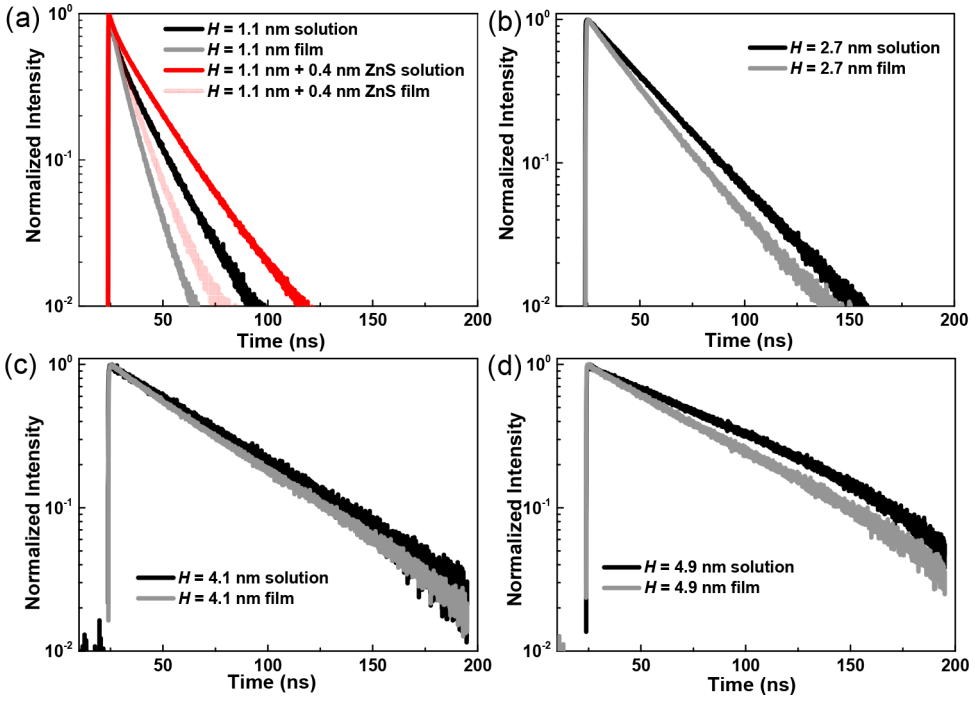

Figure 4. Solution and film PL decay of QDs. Time-resolved fluorescence decay curves of dilute toluene solutions and films of CdSe/CdS QDs with different shell thickness (H = 1.1, 2.7, 4.1, and 4.9 nm) and CdSe/CdS(1.1 nm)/ZnS(0.4 nm) QDs. The data were collected at the corresponding emission peak maxima for each sample.

$A_{\text{1st-exciton-peak}}$, which accounts for differences in QD concentration. The similarity in their first exciton bleaching confirms that we achieved very similar degree of state filling in all samples. We observed that the thin-shell QDs are spherical in shape, while thick-shell QDs are irregular. Further, a recent study reveals that shape may affect blinking behavior.[36] In our studies, however, the time dependence of the absorption bleach at the exciton peak is very similar in all samples, with slightly

DOI: 10.1021/acs.chemmater.7b00164
Chem. Mater. XXXX, XXX, XXX−XXX

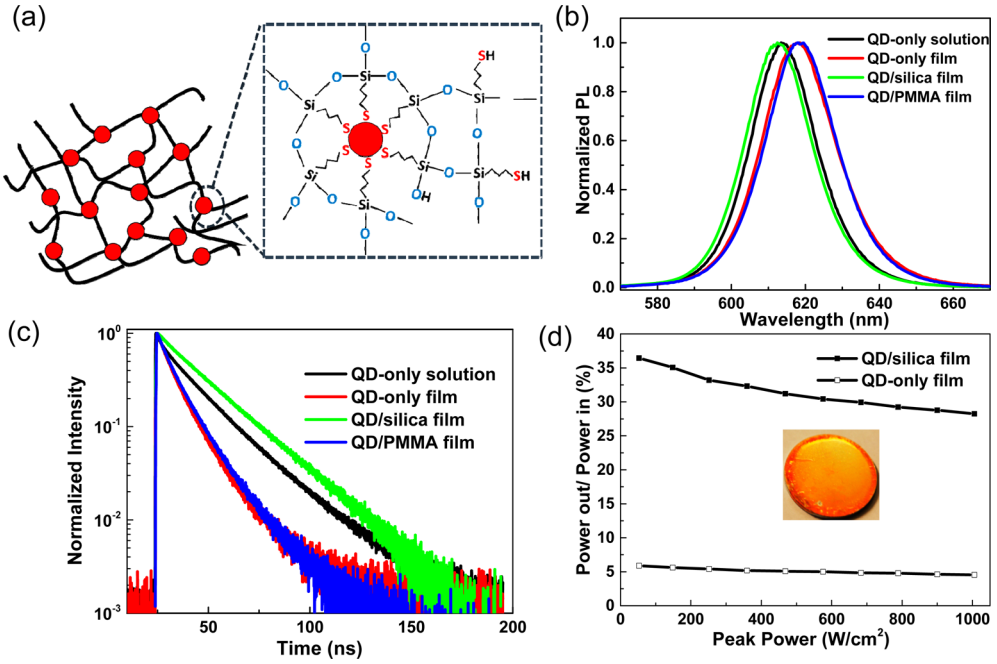

Figure 5. (a) Schematic diagram of QD/silica composites. (b) PL spectra and (c) time-resolved fluorescence decay curves for diluted toluene solution and film of CdSe/CdS(1.1 nm)/ZnS(0.4 nm) QDs, QD/silica composite film, and QD/PMMA composite film. The data for PL decay were collected at the corresponding emission peak maxima for each sample. (d) Dependence of power conversion efficiency on peak pump power for films of QDs and QD/silica composites. Inset: Digital photographs of QD/silica composite film under ambient lighting.

faster Auger decays in thick-shell samples (Figure 3b). We conclude that, in the materials studied herein, the QD shell thickness and shape do not play a dominant role in Auger recombination. We sought to confirm the underlying factors contributing to more severe PL QY loss in thicker-shelled QDs at high-power excitation. TA measurements were repeated using a 442 nm pump which is absorbed by the CdS shell. The lifetime shortens with increasing power, indicating that Auger recombination is the main decay pathway at high powers (Figure S8). At a given pump power, state filling increases with increasing shell thickness as a direct result of the larger excitation rate at the pump wavelength (Figure 3c). Correspondingly, we observe the expected faster decays in QDs with thicker shells (Figure 3d). This supports the notion that excitons accumulate more efficiently in thicker-shell QDs because higher shell absorption enables faster excitation rates, and this, in turn, results in enhanced instead of reduced Auger recombination.

Photoluminescence of QDs in Solid State. QDs with the thinnest CdS shell, however, exhibit a large decrease in PL QY when casting into films. CdSe/CdS(1.1 nm) QDs show PL QY of 46% in toluene solution, which drops to ca. 18% in the film (Table 1). This is accompanied by a red shift in the emission peak (Figure S9). In contrast, the QDs with thick shells preserve more than half of their solution PL QY in films. Energy transfer[12−14] between QDs with consequent trapping, along with exciton dissociation and reabsorption,[37] contribute to the PL reduction in the solid state. The thicker shell forms a large barrier that prevents energy and carrier transfer, resulting in a smaller drop in PL QY when concentrating from a dilute solution into a solid film.

To further confirm the role of energy transfer, we obtained time-resolved PL for dilute solutions and films of QDs with different shell thicknesses. These measurements were made using time-correlated single-photon counting spectroscopy (Figure 4). The PL decay dynamics for all QDs in solid films are faster than their corresponding solution samples, with the largest variation observed for the thinnest shells (H = 1.1 nm) (Figure 4a). The decay curves were fitted using a single exponential decay function (Table 1). The results indicate that significant energy transfer—which is faster than the radiative recombination—exists in thin-shell QD films,[2−13] leading to the reduction in PL efficiency.

Enhanced PL Performance of Thin-Shell QDs in Matrix. The above investigations suggest that thin CdS-shelled QDs can efficiently increase the pump-power threshold of Auger recombination. This results in the best-retained solution PL QY in kW/cm^2 operating regime. However, these QDs suffer from poor solid-state PL performance due to distance-dependent nonradiative energy transfer. In order to overcome this effect, the introduction of a spacer between QDs is desirable to increase interdot distance. Herein, we employed a strategy to separate the QDs by embedding them in a transparent silica matrix, greatly reducing interdot energy transfer. Silica is of interest due to its excellent optical properties and stability, as well as good compatibility with silicone resin often used in device encapsulation. Silica-coated QD nano/microparticles have been well developed via the Stöber method and reverse microemulsion process, but suffer from reduced PL compared to that of original QDs.[38,39] Films and monoliths of QDs embedded in silica matrix have also been explored, with film PL QYs reported being in the 18%−41% range.[20,40,41] Recently, with the use of 6-mercaptohexanol as a covalent linker between QDs and silica, researchers realized red light-emitting monoliths with external quantum efficiency of up to 63% at low pump power.[42] Here we utilized (3-mercaptopropyl)trimethoxysilane (MPS) as the exchange ligand and as the sol−gel condensation precursor for the silica matrix (Figure 5a). The introduction of covalent bonds between the surface of the QDs and the matrix was expected

DOI: 10.1021/acs.chemmater.7b00164
Chem. Mater. XXXX, XXX, XXX−XXX

to improve the compatibility of the composites and lead to a uniform dispersion of the QDs in the matrix.[15−17,42]

CdSe/CdS(1.1 nm)/ZnS(0.4 nm) QDs with the highest absolute PL QY of the solution at high pump powers were chosen to fabricate the solid phosphor. Given that the thin CdS shell (e.g., H = 1.1) could not provide sufficient exciton confinement for CdSe core, owing to its small band offset at the conduction band, we grew an extra thin ZnS shell. This provided exciton confinement and better passivation for achieving higher solution PL QY. Since the photon energy (2.81 eV) applied in this case is insufficient to excite the absorption of ZnS shell (bulk E_g = 3.54 eV), the excitonic occupancy, power dependency, and excitation-dependent decay trace are not affected by the additionally grown ZnS shell (Figure 1b, Figures 2−4). The growth of a thin ZnS shell with a wide bandgap enables QDs to maintain a high PL QY during the subsequent ligand exchange process.[43,44] The doubly shelled QDs were treated with MPS for surface ligand exchange. The success of ligand exchange is confirmed by verifying the solubility of QDs in different solvents. The initial QDs are readily dispersed in THF but are insoluble in ethanol. In contrast, the QDs after ligand exchange with MPS are soluble in ethanol but insoluble in THF and in hexane. IR spectra further confirm the success of ligand exchange of OA with MPA (Figure S10). Then QD/silica composites were prepared via hydrolytic condensation and cross-linking reactions, resulting in a uniform distribution of the QDs in the silica matrix, with good separation of QDs and increased interdot distance (see TEM image in Figure S11). As a control, we also fabricated QDs in a poly(methyl methacrylate) (PMMA) matrix by simple mixing.

The QD/silica composite films exhibit significantly superior PL properties compared with those of the QD-only films and QD/PMMA composite films (Table 1, Figure 5b). The PL QY of CdSe/CdS(1.1 nm)/ZnS(0.4 nm) QDs sharply decreases from 60% in solution to 20% in the solid state, along with a red shift from 614 to 618 nm in PL peak, suggesting QD aggregation and short interdot distance. A similar trend is observed in the QD/PMMA composite films, suggesting that QDs do not distribute uniformly in the PMMA matrix due to the lack of chemical bonds between QDs and the polymer matrix. In contrast, the QD/silica composite films display enhanced PL QY of 65%. The PL decay for QD/silica composite films become much slower compared to the QD-only films and QD/PMMA composite films, indicating elimination of energy transfer for QDs in the silica matrix (Figure 5c, Table 1). It is worth noting that the PL lifetime of the QD/silica composite films is even longer than that of the dilute solution samples of QDs, suggesting that improved surface passivation has been achieved when the QDs are incorporated into the silica matrix. We attribute the improvement in film PL QYs for QDs in silica matrix to improved surface passivation combined with good separation of QDs via the effect of the covalently bonded silica network,[16,17,24,42] and the dielectric confinement effect.[45] Continued effort is required to clarify the factors for the improvement of film PL QYs of QDs.

Finally, the power conversion efficiency of QD/silica composites was investigated under high excitation powers. A QD/silica composite film was formed on a reflective aluminum mirror (inset in Figure 5d). For comparison, a QD-only film was prepared as a control. The films were excited using a high-power pulsed laser diode system at a wavelength of 442 nm, and the emitted light was collected using a lens system directed to an OPHIR PD300-3W photodiode with a 9 mm aperture. Both film samples show more than 70% absorption at 442 nm (Figure S12) and exhibit similar trends in the relative PL QY as a function of pump intensity (Figure S13). The absolute power conversion efficiency of QD/silica composite film reaches 36% at low excitation intensities and retains >80% of its initial value to yield an absolute power conversion efficiency of 28% under 1 kW/cm^2 excitation intensities (Figure 5d). In contrast, QD-only film yields 4.5% at these intensities. After 80 min of stability testing at 2.5 kW/cm^2, the obtained QD/silica composites retain 97% of the initial efficiency (Figure S14).

CONCLUSIONS

This work demonstrates a new route to realizing high PL performance for QD films under high power excitation. It exploits a combination of reduced multiexciton Auger recombination through thin-shell design, and avoidance of energy transfer via incorporation into a transparent, solid-state dot-dispersing matrix. The work demonstrates the impact of shell thickness on Auger recombination in QDs. While biexciton Auger recombination rates do slow with thicker shells, under the same external pump power (a condition more relevant for device applications), overall Auger recombination is in fact enhanced due to the formation of higher order multiexcitons. Decreasing the shell thickness allows better retention of the original PL QY at high-power excitation. A thin ZnS layer was grown on thin-shell QDs to provide better passivation and exciton confinement while limiting the amount of absorption at the pump wavelength. To overcome severe PL quenching in films of QDs with thin shells, we deployed transparent matrices that isolate the QDs and avoid energy transfer among them. Leveraging these observations and techniques, we present a functional platform that enables QDs to be included in high-power applications and potentially replace existing phosphor technology for pure color and bright light emission purposes.

ASSOCIATED CONTENT

Supporting Information

The Supporting Information is available free of charge on the ACS Publications website at DOI: 10.1021/acs.chemmater.7b00164.

UV−vis absorption, PL, and IR spectra, TEM images, TA spectroscopy, pump-power-dependent relative PL QY, and PL stability data (PDF)

AUTHOR INFORMATION

Corresponding Author

*E-mail: ted.sargent@utoronto.ca.

ORCID

Cai-Feng Wang: 0000-0003-4667-2120
Oleksandr Voznyy: 0000-0002-8656-5074
Kristopher Bicanic: 0000-0002-3020-4093

Author Contributions

†C.-F.W and F.F. contributed equally to the work.

Notes

The authors declare no competing financial interest.

DOI: 10.1021/acs.chemmater.7b00164
Chem. Mater. XXXX, XXX, XXX−XXX

■ ACKNOWLEDGMENTS

This work was supported by the Natural Sciences and Engineering Research Council (NSERC) of Canada. It was also supported by Jiangsu Overseas Research & Training Program for University Prominent Young & Middle-aged Teachers and Presidents. The authors thank D. Kopilovic, E. Palmiano, and R. Wolowiec for their technical help on this work.

■ REFERENCES

(1) Shirasaki, Y.; Supran, G. J.; Bawendi, M. G.; Bulovic, V. Emergence of Colloidal Quantum-Dot Light-Emitting Technologies. *Nat. Photonics* **2013**, *7*, 13−23.

(2) Coe-Sullivan, S.; Liu, W. H.; Allen, P.; Steckel, J. S. Quantum Dots for LED Downconversion in Display Applications. *ECS J. Solid State Sci. Technol.* **2013**, *2*, R3026−R3030.

(3) Klimov, V. I.; Mikhailovsky, A. A.; McBranch, D. W.; Leatherdale, C. A.; Bawendi, M. G. Quantization of Multiparticle Auger Rates in Semiconductor Quantum Dots. *Science* **2000**, *287*, 1011−1013.

(4) Park, Y. S.; Malko, A. V.; Vela, J.; Chen, Y.; Ghosh, Y.; García-Santamaría, F.; Hollingsworth, J. A.; Klimov, V. I.; Htoon, H. Near-Unity Quantum Yields of Biexciton Emission from CdSe/CdS Nanocrystals Measured Using Single-Particle Spectroscopy. *Phys. Rev. Lett.* **2011**, *106*, 187401.

(5) Klimov, V. I. Spectral and Dynamical Properties of Multiexcitons in Semiconductor Nanocrystals. *Annu. Rev. Phys. Chem.* **2007**, *58*, 635−673.

(6) Robel, I.; Gresback, R.; Kortshagen, U.; Schaller, R. D.; Klimov, V. I. Universal Size-Dependent Trend in Auger Recombination in Direct-Gap and Indirect-Gap Semiconductor Nanocrystals. *Phys. Rev. Lett.* **2009**, *102*, 177404.

(7) Rabouw, F. T.; Lunnemann, P.; van Dijk-Moes, R. J.; Frimmer, M.; Pietra, F.; Koenderink, A. F.; Vanmaekelbergh, D. Reduced Auger Recombination in Single CdSe/CdS Nanorods by One-Dimensional Electron Delocalization. *Nano Lett.* **2013**, *13*, 4884−4892.

(8) Cragg, G. E.; Efros, A. L. Suppression of Auger Processes in Confined Structures. *Nano Lett.* **2010**, *10*, 313−317.

(9) García-Santamaría, F.; Brovelli, S.; Viswanatha, R.; Hollingsworth, J. A.; Htoon, H.; Crooker, S. A.; Klimov, V. I. Breakdown of Volume Scaling in Auger Recombination in CdSe/CdS Heteronanocrystals: The Role of the Core−Shell Interface. *Nano Lett.* **2011**, *11*, 687−693.

(10) Park, Y. S.; Bae, W. K.; Padilha, L. A.; Pietryga, J. M.; Klimov, V. I. Effect of the Core/Shell Interface on Auger Recombination Evaluated by Single-Quantum-Dot Spectroscopy. *Nano Lett.* **2014**, *14*, 396−402.

(11) Bae, W. K.; Park, Y. S.; Lim, J.; Lee, D.; Padilha, L. A.; McDaniel, H.; Robel, I.; Lee, C.; Pietryga, J. M.; Klimov, V. I. Controlling the Influence of Auger Recombination on the Performance of Quantum-Dot Light-Emitting Diodes. *Nat. Commun.* **2013**, *4*, 2661.

(12) Pal, B. N.; Ghosh, Y.; Brovelli, S.; Laocharoensuk, R.; Klimov, V. I.; Hollingsworth, J. A.; Htoon, H. 'Giant' CdSe/CdS Core/Shell Nanocrystal Quantum Dots As Efficient Electroluminescent Materials: Strong Influence of Shell Thickness on Light-Emitting Diode Performance. *Nano Lett.* **2012**, *12*, 331−336.

(13) Khon, E.; Lambright, S.; Khon, D.; Smith, B.; O'Connor, T.; Moroz, P.; Imboden, M.; Diederich, G.; Perez-Bolivar, C.; Anzenbacher, P.; Zamkov, M. Inorganic Solids of CdSe Nanocrystals Exhibiting High Emission Quantum Yield. *Adv. Funct. Mater.* **2012**, *22*, 3714−3722.

(14) Lunz, M.; Bradley, A. L.; Chen, W. Y.; Gerard, V. A.; Byrne, S. J.; Gun'ko, Y. K.; Lesnyak, V.; Gaponik, N. Influence of Quantum Dot Concentration on Forster Resonant Energy Transfer in Monodispersed Nanocrystal Quantum Dot Monolayers. *Phys. Rev. B: Condens. Matter Mater. Phys.* **2010**, *81*, 205316.

(15) Tomczak, N.; Jańczewski, D.; Han, M.; Vancso, G. J. Designer Polymer−Quantum Dot Architectures. *Prog. Polym. Sci.* **2009**, *34*, 393−430.

(16) Cao, X.; Li, C. M.; Bao, H.; Bao, Q.; Dong, H. Fabrication of Strongly Fluorescent Quantum Dot−Polymer Composite in Aqueous Solution. *Chem. Mater.* **2007**, *19*, 3773−3779.

(17) Yang, S.; Wang, C. F.; Chen, S. Interface-Directed Assembly of One-Dimensional Ordered Architecture from Quantum Dots Guest and Polymer Host. *J. Am. Chem. Soc.* **2011**, *133*, 8412−8415.

(18) Otto, T.; Müller, M.; Mundra, P.; Lesnyak, V.; Demir, H. V.; Gaponik, N.; Eychmüller, A. Colloidal Nanocrystals Embedded in Macrocrystals: Robustness, Photostability, and Color Purity. *Nano Lett.* **2012**, *12*, 5348−5354.

(19) Tetsuka, H.; Ebina, T.; Mizukami, F. Highly Luminescent Flexible Quantum Dot−Clay Films. *Adv. Mater.* **2008**, *20*, 3039−3043.

(20) Lita, A.; Washington, A. L.; van de Burgt, L.; Strouse, G. F.; Stiegman, A. E. Stable Efficient Solid-State White-Light-Emitting Phosphor with a High Scotopic/Photopic Ratio Fabricated from Fused CdSe−Silica Nanocomposites. *Adv. Mater.* **2010**, *22*, 3987−3991.

(21) Meinardi, F.; Colombo, A.; Velizhanin, K. A.; Simonutti, R.; Lorenzon, M.; Beverina, L.; Viswanatha, R.; Klimov, V. I.; Brovelli, S. Large-Area Luminescent Solar Concentrators based on`Stokes-Shift-Engineered' Nanocrystals in a Mass-Polymerized PMMA Matrix. *Nat. Photonics* **2014**, *8*, 392−399.

(22) Yu, W. W.; Qu, L.; Guo, W.; Peng, X. Experimental Determination of the Extinction Coefficient of CdTe, CdSe, and CdS Nanocrystals. *Chem. Mater.* **2003**, *15*, 2854−2860.

(23) Chen, O.; Zhao, J.; Chauhan, V. P.; Cui, J.; Wong, C.; Harris, D. K.; Wei, H.; Han, H.-S.; Fukumura, D.; Jain, R. K.; Bawendi, M. G. Compact High-Quality CdSe−CdS Core−Shell Nanocrystals with Narrow Emission Linewidths and Suppressed Blinking. *Nat. Mater.* **2013**, *12*, 445−451.

(24) Gerion, D.; Pinaud, F.; Williams, S. C.; Parak, W. J.; Zanchet, D.; Weiss, S.; Alivisatos, A. P. Synthesis and Properties of Biocompatible Water-Soluble Silica-Coated CdSe/ZnS Semiconductor Quantum Dots. *J. Phys. Chem. B* **2001**, *105*, 8861−8871.

(25) She, C.; Fedin, I.; Dolzhnikov, D. S.; Demortière, A.; Schaller, R. D.; Pelton, M.; Talapin, D. V. Low-Threshold Stimulated Emission Using Colloidal Quantum Wells. *Nano Lett.* **2014**, *14*, 2772−2777.

(26) Li, J. J.; Wang, Y. A.; Guo, W.; Keay, J. C.; Mishima, T. D.; Johnson, M. B.; Peng, X. Large-Scale Synthesis of Nearly Monodisperse CdSe/CdS Core/Shell Nanocrystals Using Air-Stable Reagents via Successive Ion Layer Adsorption And Reaction. *J. Am. Chem. Soc.* **2003**, *125*, 12567−12575.

(27) Cirillo, M.; Aubert, T.; Gomes, R.; Van Deun, R.; Emplit, P.; Biermann, A.; Lange, H.; Thomsen, C.; Brainis, E.; Hens, Z. Flash" Synthesis of CdSe/CdS Core−Shell Quantum Dots. *Chem. Mater.* **2014**, *26*, 1154−1160.

(28) Qin, H.; Niu, Y.; Meng, R.; Lin, X.; Lai, R.; Fang, W.; Peng, X. Single-Dot Spectroscopy of Zinc-Blende CdSe/CdS Core/Shell Nanocrystals: Nonblinking and Correlation with Ensemble Measurements. *J. Am. Chem. Soc.* **2014**, *136*, 179−187.

(29) Christodoulou, S.; Vaccaro, G.; Pinchetti, V.; De Donato, F.; Grim, J. Q.; Casu, A.; Genovese, A.; Vicidomini, G.; Diaspro, A.; Brovelli, S.; Manna, L.; Moreels, I. Synthesis of Highly Luminescent Wurtzite CdSe/CdS Giant-Shell Nanocrystals Using a Fast Continuous Injection Route. *J. Mater. Chem. C* **2014**, *2*, 3439−3447.

(30) Cui, J.; Beyler, A. P.; Coropceanu, I.; Cleary, L.; Avila, T. R.; Chen, Y.; Cordero, J. M.; Heathcote, S. L.; Harris, D. K.; Chen, O.; Cao, J.; Bawendi, M. G. Evolution of the Single-Nanocrystal Photoluminescence Linewidth with Size and Shell: Implications for Exciton-Phonon Coupling and the Optimization of Spectral Linewidths. *Nano Lett.* **2016**, *16*, 289−296.

(31) de Mello, J. C.; Wittmann, H. F.; Friend, R. H. An Improved Experimental Determination of External Photoluminescence Quantum Efficiency. *Adv. Mater.* **1997**, *9*, 230−232.

(32) Kambhampati, P. Multiexcitons in Semiconductor Nanocrystals: A Platform for Optoelectronics at High Carrier Concentration. *J. Phys. Chem. Lett.* **2012**, *3*, 1182−1190.

(33) Kambhampati, P. Unraveling the Structure and Dynamics of Excitons in Semiconductor Quantum Dots. *Acc. Chem. Res.* **2011**, *44*, 1−13.

DOI: 10.1021/acs.chemmater.7b00164
Chem. Mater. XXXX, XXX, XXX−XXX

(34) Tyagi, P.; Kambhampati, P. False Multiple Exciton Recombination and Multiple Exciton Generation Signals in Semiconductor Quantum Dots Arise from Surface Charge Trapping. *J. Chem. Phys.* **2011**, *134*, 094706.
(35) Kambhampati, P. On the Kinetics and Thermodynamics of Excitons at the Surface of Semiconductor Nanocrystals: Are There Surface Excitons? *Chem. Phys.* **2015**, *446*, 92−107.
(36) Tan, R.; Yuan, Y.; Nagaoka, Y.; Eggert, D.; Wang, X.; Thota, S.; Guo, P.; Yang, H.; Zhao, J.; Chen, O. Monodisperse Hexagonal Pyramidal and Bipyramidal Wurtzite CdSe-CdS Core−Shell Nanocrystals. *Chem. Mater.* **2017**, *29*, 4097−4108.
(37) Coropceanu, I.; Bawendi, M. G. Core/shell quantum dot based luminescent solar concentrators with reduced reabsorption and enhanced efficiency. *Nano Lett.* **2014**, *14*, 4097−4101.
(38) Nann, T.; Mulvaney, P. Single Quantum Dots in Spherical Silica Particles. *Angew. Chem., Int. Ed.* **2004**, *43*, 5393−5396.
(39) Koole, R.; van Schooneveld, M. M.; Hilhorst, J.; de Mello Donegá, C.; Hart, D. C.; van Blaaderen, A.; Vanmaekelbergh, D.; Meijerink, A. On the Incorporation Mechanism of Hydrophobic Quantum Dots in Silica Spheres by a Reverse Microemulsion Method. *Chem. Mater.* **2008**, *20*, 2503−2512.
(40) Li; Murase, N. Synthesis of Highly Luminescent Glasses Incorporating CdTe Nanocrystals through Sol−Gel Processing. *Langmuir* **2004**, *20*, 1−4.
(41) Yang, P.; Li, C. L.; Murase, N. Highly Photoluminescent Multilayer QD−Glass Films Prepared by LbL Self-Assembly. *Langmuir* **2005**, *21*, 8913−8917.
(42) Jun, S.; Lee, J.; Jang, E. Highly Luminescent and Photostable Quantum Dot-Silica Monolith and Its Application to Light-Emitting Diodes. *ACS Nano* **2013**, *7*, 1472−1477.
(43) Blackman, B.; Battaglia, D.; Peng, X. Bright and Water-Soluble Near IR-Emitting CdSe/CdTe/ZnSe Type-II/Type-I Nanocrystals, Tuning the Efficiency and Stability by Growth. *Chem. Mater.* **2008**, *20*, 4847−4853.
(44) Munro, A. M.; Jen-La Plante, I.; Ng, M. S.; Ginger, D. S. Quantitative Study of the Effects of Surface Ligand Concentration on CdSe Nanocrystal Photoluminescence. *J. Phys. Chem. C* **2007**, *111*, 6220−6227.
(45) Wang, Y.; Herron, N. Nanometer-Sized Semiconductor Clusters - Materials Synthesis, Quantum Size Effects, and Photophysical Properties. *J. Phys. Chem.* **1991**, *95*, 525−532.

DOI: 10.1021/acs.chemmater.7b00164
Chem. Mater. XXXX, XXX, XXX−XXX